Smart Structures and Systems, Vol. 9, No. 6 (2012) 535-547
DOI: http://dx.doi.org/10.12989/sss.2012.9.6.535

Flexible tactile sensor array for foot pressure mapping system in a biped robot

Cheng-Hsin Chuang*[1], Yi-Rong Liou[1] and Ming-Yuan Shieh[2]

[1]Department of Mechanical Engineering & Institute of Nanotechnology, Southern Taiwan University, Tainan 71005, Taiwan
[2]Department of Electrical Engineering, Southern Taiwan University, Tainan 71005, Taiwan

(Received August 1, 2011, Revised May 17, 2012, Accepted May 22, 2012)

Abstract. Controlling the balance of motion in a context involving a biped robot navigating a rugged surface or a step is a difficult task. In the present study, a 3×5 flexible piezoelectric tactile sensor array is developed to provide a foot pressure map and zero moment point for a biped robot. We introduce an innovative concept involving structural electrodes on a piezoelectric film in order to improve the sensitivity. The tactile sensor consists of a polymer piezoelectric film, *PVDF*, between two patterned flexible print circuit substrates (*FPC*). Additionally, a silicon rubber bump-like structure is attached to the *FPC* and covered by a polydimethylsiloxane (*PDMS*) layer. Experimental results show that the output signal of the sensor exhibits a linear behavior within 0.2 N ~ 9 N, while its sensitivity is approximately 42 mV/N. According to the characteristic of the tactile sensor, the readout module is designed for an in-situ display of the pressure magnitudes and distribution within 3×5 taxels. Furthermore, the trajectory of the zero moment point (*ZMP*) can also be calculated by this program. Consequently, our tactile sensor module can provide the pressure map and *ZMP* information to the in-situ feedback to control the balance of moment for a biped robot.

Keywords: tactile sensor; piezoelectric; foot pressure; biped robot

1. Introduction

Walking is the most common mode by which people move from one place to another. It is easy for humans to maintain their balance, whether they are walking on a rugged surface, a sloping surface or a stairway, due to feedback from the vestibular system in the inner ear which is required for clear vision and the projections to the muscles that control our posture and are necessary to keep us upright (Mergner *et al.* 2009). However, this is currently a difficult task for even the most advanced biped robot because of a lack of sensory feedback which allows the robot to adjust its center of gravity and maintain its balance while in motion. Recently, the concept of the zero moment point (*ZMP*) (Vukobratovic and Borovac 2004, Kalamdani *et al.* 2006) has been used to reduce the overturning moment, which is the point with respect to the dynamic reaction force at the contact of the foot with the ground without producing any moment. Therefore, in order to maintain a satisfactory dynamic postural stability for a humanoid robot, the magnitude and distribution patterns of foot pressure under dynamic variations are crucial for the calculation of *ZMP* (Park

*Corresponding author, Associate Professor, E-mail: chchuang@mail.stut.edu.tw

2003). Although the foot pressure mapping system has been available for medical applications or shoe designs (Cavanagh *et al.* 1992), a real-time and low-cost flexible sensor for the feedback of foot pressure is sorely needed in order to advance robotic motion control.

Early foot pressure measurements employed ink for the imprinting of pressure distributions of the foot. Welton (1992) also used this method to imprint foot pressure and transferred the pattern into a normal force value. Currently, foot pressure measuring systems can be divided into the force plate system (MacWilliams *et al.* 2000) and the placed sensor system (Zhu *et al.* 1990). For the force plate system, the main structure is a flat platform with multi-axial force sensors which is usually fixed on the surface or placed on the ground to measure the reaction force between the foot and the ground. Although the single stance phase of gait is possible to inversely calculate based on the ground reaction forces (*GRFs*), however, the number of force plates limits the number of consecutive strides that can be recorded as walking (Forner-Cordero *et al.* 2006). On the other hand, a placed sensor system means there is an embedded sensor on the bottom of the foot for continuous measurement of the reaction force in motion. Therefore, a portable placed sensor system is more likely to fulfill the requirements for the foot pressure measurement of a biped robot. Two kinds of sensors have been utilized for the placed sensor system: Force Sensing Resistor (*FSR*) (Interlink Electronics Inc. 2011) and F-Scan (Tekscan Inc. 2011). The *FSR* is a single-point pressure measurement device based on a piezoresistive mechanism. Though *FSR* is simple and user-friendly, the point size cannot satisfy the requirement of resolution for a foot pressure mapping system, and the wiring issue is also complicated because of the multi-sensor array. In addition, the output signal depends on the resistance change of conductive rubber in response to pressure, which usually exhibits non-linear characteristics in the sensing range. Hence, additional calibration is needed (Yip and Prieto 1996). F-Scan is a piezoresistive-type pressure measurement device with a mapping function. The F-Scan system has been implemented for in-shoe pressure monitoring for clinical purposes; however, there is considerable hysteresis, and the creep behavior also needs to be dealt with. For example, when 500 kPa pressure was applied on the F-Scan for 15 minutes, the output value declined by a margin of 19% (Woodbum and Helliwell 1997). In contrast with the piezoelectric-type pressure sensor, a polymer-based piezoelectric material, polyvinylidene fluoride (*PVDF*), has exhibited some beneficial characteristics, such as flexible mechanics, good linearity of output voltage under dynamic loading and a low-hysteresis effect for cyclic pressure change. Thus, *PVDF*-based tactile sensors have been investigated for monitoring dynamic contact force, such as grasping force and slippage detection (Saito *et al.* 2006, Teshigawara *et al.* 2008, Chuang *et al.* 2009, Qasaimeh *et al.* 2009). However, a piezoelectric-type tactile sensor for mapping foot pressure on a moving robot has not been investigated yet. In the present study, we introduced a bump-like structure on the corresponding electrode to increase the output signals of the piezoelectric tactile sensor, and to avoid the low sensitivity and noise problems which are commonly found in *PVDF*-based sensors. Due to the bump-like structure can be regarded as a force transferring component to the corresponding electrode, the combination of bump-like structure and electrode was so-called as “structural electrode” (Chuang *et al.* 2008). Furthermore, we used micromachining technology (*MEMS*) to fabricate a 3×5 tactile sensor array for foot pressure mapping. For the aspect of the system, a read-out circuit module and a computer-based program for visualized pressure mapping and zero moment point calculation were also integrated with the tactile sensor so that the robot could receive real-time feedback from this foot pressure mapping system so as to control its balance of motion.

2. Tactile sensor with structural electrode array

The flexible 3×5 tactile sensor array consisted of two patterned flexible printed circuits (*FPC*) sandwiching a polymer piezoelectric film (*PVDF*), and 15 bump-like structures made of silicone rubber attached to the *FPC* surface and packaged with *PDMS* material, as shown in Fig. 1. Within the robot foot area (53 mm×48 mm), total 15 taxels can be monitored by our tactile sensor array, which was sufficient for the calculation of *ZMP* in our case. However, if one wants to increase the density of taxels, some challenges need to be solved as downsizing the electrode size and spacing, for instance, low signal output, cross-talk effect and wiring issue, etc. By adding the bump-like structure to the electrode patterned on the *FPC*, the sensitivity of the piezoelectric-type tactile sensor could be improved; this was the so-called structural electrode which replaced the thin-film electrode in the traditional piezoelectric sensor (Yu *et al.* 2003). Contrary to what occurs with a thin-film electrode, the effect of stress concentration could be generated in the piezoelectric material when the contact force was transferred through the bump-like structures instead of through uniform contact with the piezoelectric material. The induced charge of the piezoelectric material was increased due to the stress concentrated underneath the bump-like structures. Moreover, the tactile sensor was essentially flexible and easily attached to any uneven surface, such as robotic feet. In our previous work (Chuang *et al.* 2008, 2009), the electrode layer was directly deposited on *PVDF* film by a thermal evaporator, then, the electrodes were patterned by metal wet etch. Due to the high temperature during thermal evaporation could affect the piezoelectricity of *PVDF*; we modified the process of electrode patterning. Instead of directly patterning the electrodes on *PVDF* material, the

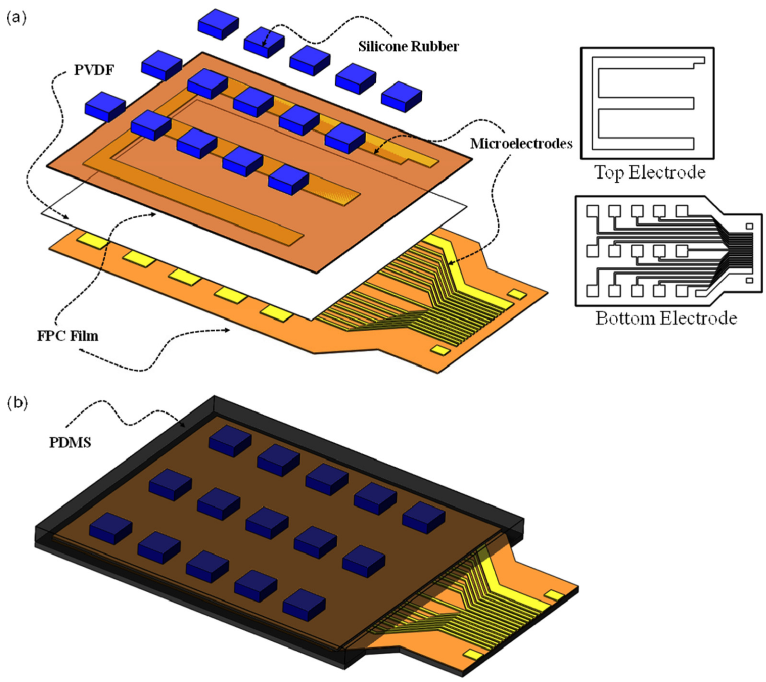

Fig. 1 The structure of a 3×5 flexible tactile sensor array, and its dimensions in length, width and height: 53 mm, 48 mm and 4 mm, respectively. (a) The structure and electrode design of the sensor separated layer by layer and (b) the finished sensor after packaging by *PDMS* material

microelectrodes array was patterned on both top and bottom *FPC* and the bump-like structure was discretely aligned and bonded on the top of *FPC* for better signal isolation and less cross-talk effect. Consequently, the present flexible tactile sensor has the potential to be mass manufactured using a low-temperature process.

3. Numerical simulation

3.1 3D Model of the tactile sensor with single structural electrode

A 3D model of the tactile sensor with a single structural electrode was established and calculated based on commercial finite element software (*ABAQUS*). All dimensions and material properties of the simulation model are illustrated in Fig. 2 and Table 1, respectively. In the simulations, the

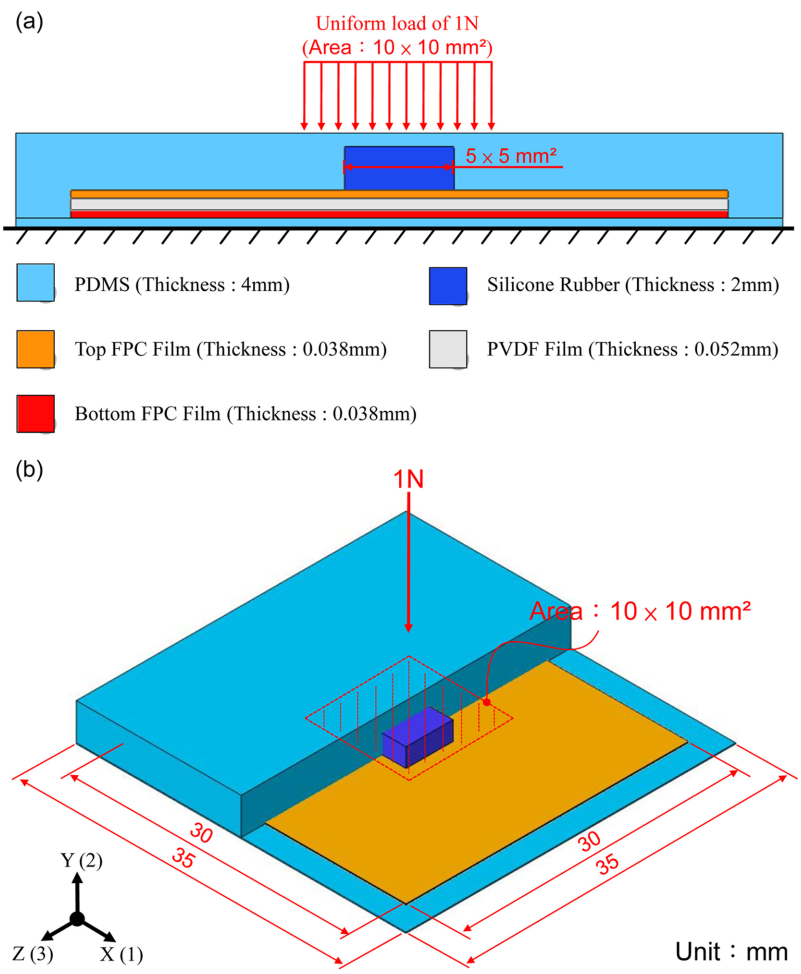

Fig. 2 The 3D simulation model of the tactile sensor with a single structural electrode: (a) the cross section and thickness of each layer and (b) the domain of model and loading conditions

Table 1 Material properties for numerical simulation

	PVDF	bump-like structure	*FPC* Film	*PDMS*
Density (kg/m^3)	1780	1570	1353	1083
Young's modulus (MPa)	3000	5.45	2500	1
Poisson's ratio	0.35	0.45	0.34	0.45
Dielectric constant (Farad/m)	11×10^{-10}			
d_{211}, d_{233} (m/Volt)	23×10^{-12}			
d_{222} (m/Volt)	-33×10^{-12}			

external force of 1 N was set to load on the tactile sensor top surface within a square of 10×10 mm^2, and the bottom surface was set as a fixed-end boundary condition. Note that all the interfaces between different materials were set as perfect bonding conditions, i.e., the stress and strain were continuous at the interface surface. These boundary conditions were analogous to the experimental setup for characterization of the sensitivity of the sensor. The mesh of the 3D model was established by 8-node hexahedral elements, and the total element number as determined by a convergence test was around 100,000. When the contact force was acting on the surface of the tactile sensor, the inner bump-like structure and outside packaging layer were regarded as the force transmission components to the sensing material (*PVDF*). Therefore, the material selection of the bump-like structure and the packaging layer would have significant influence on the stress distribution as well as the sensor output. In this study, the effect of the Young's Modulus ratio between the bump-like structure material and the packaging layer on the sensor output was parametrically investigated for the enhancement of sensitivity.

3.2 Simulation results

The contour of electric potential on the piezoelectric film as 1 N loaded on the tactile sensor is illustrated in Fig. 3(a), and a cross-sectional profile of the electric potential is plotted in Fig. 3(b). The results indicated that there was a plateau region of electrical potential corresponding to the stress concentration underneath the silicone rubber bump-like structure, although the applied loading was uniform on the sensor surface. Furthermore, two peak values of electric potential occurred at the edge of the bump-like structure due to a great deformation could be induced on the *PVDF* film. In general, the cross-talk effect was to be avoided as we wanted to exactly identify the image of the contact area when an object or a force came into contact with the tactile sensor. Cross-talk refers to zero contact at the taxel, but it still gathers the output signal due to the influence of other neighboring taxels. As shown in Fig. 3(b), the electric potential could still be gathered outside the loading area, as indicated by the influence range; therefore, the cross-talk effect had to take into account the spacing between two bump-like structures or the isolation of the ground electrode on the backside of the sensor. In addition, the influence range was about 5 mm away from the loading area as indicated in Fig. 3(b), thus, the minimum spacing between two neighboring taxels is 5 mm which value was also utilized in our sensor design. As well as the sensitivity enhancement due to the bump-like structure, we also improved the sensitivity by altering the packaging material. As shown in Fig. 3(c), when the Young's Modulus ratio between the bump-like structure material and the packaging material increased, the output voltages also increased. Thus, a combination of a

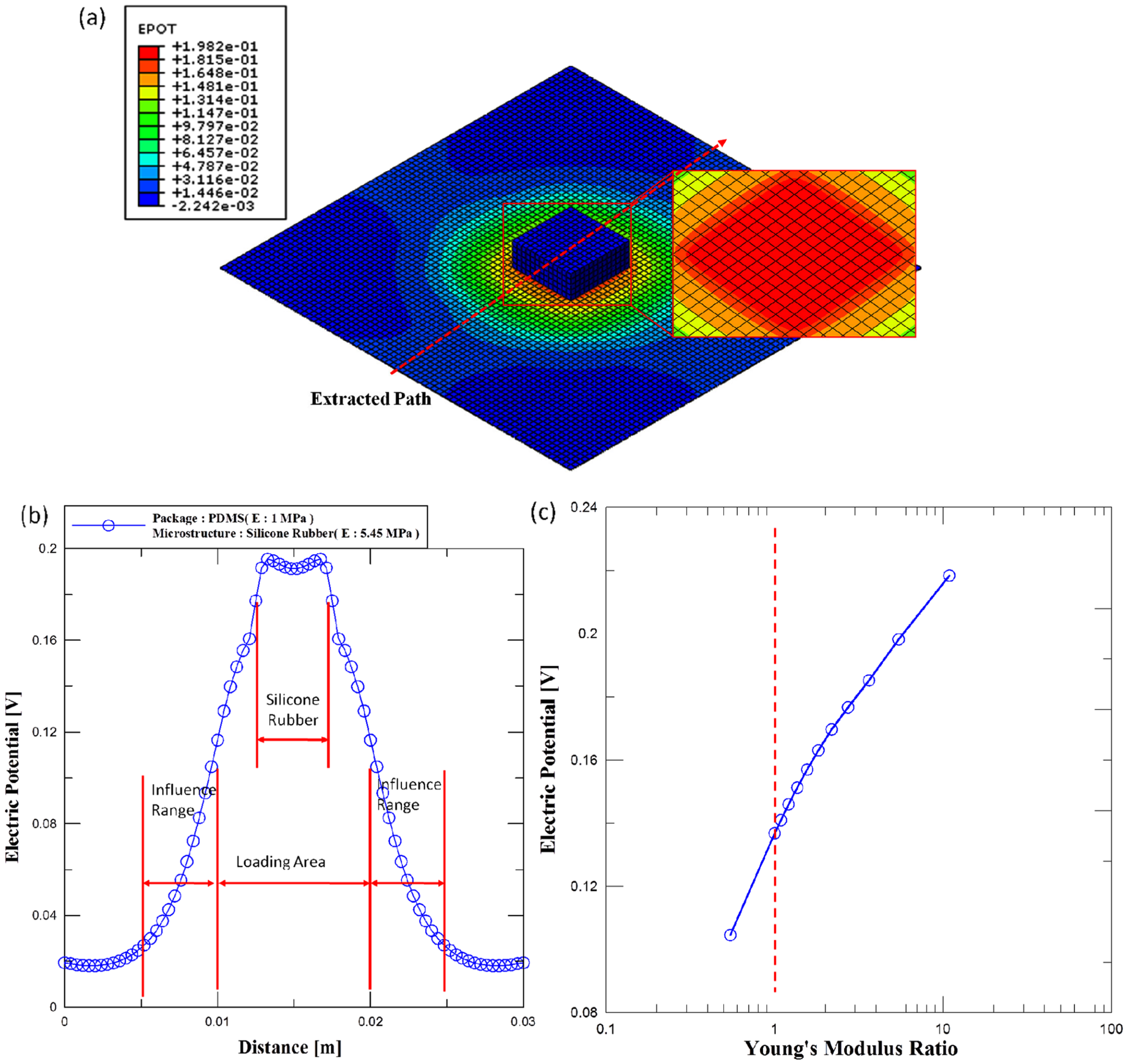

Fig. 3 Simulation results of tactile sensor with a single silicone rubber bump-like structure (E=5.45 MPa) and packaged by *PDMS* (E=1 MPa) as applied 1 N: (a) contour of electric potential on the *PVDF* surface, (b) profile of electric potential along an extracted path as indicated in (a) and (c) the output voltages versus the ratios of Young's Modulus between the inside bump-like structure material and the outside package material

harder bump-like structure and a softer packaging layer created higher sensitivity because most of the contact force was transferred by the stiffer bump-like structure instead of the pliant packaging material. However, these results are true based on the uniform contact force on the sensor surface. Therefore, when the rigidity of contacted object is similar or softer than packaging layer, the contact force could be uneven on the sensor surface so that a smaller voltage output is expected as the sensor packaged by a soft material.

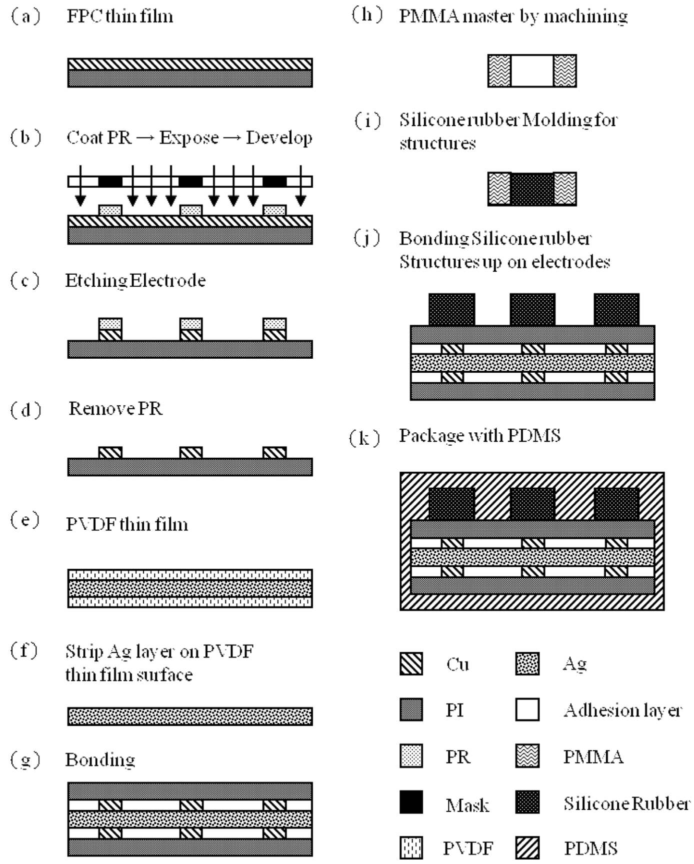

Fig. 4 The fabrication processes of the 3×5 tactile sensor array

4. Sensor fabrication

The fabrication process of the flexible tactile sensor array is shown in Fig. 4; the details are described as follows:

i. A commercial flexible printed circuit spin coated a positive photoresist S1813, then a photomask of distributed electrodes design was used to pattern the microelectrode array on *FPC* by standard photolithography, as referred to in Figs. 4(a) and (b).

ii. The patterned photoresist was then used as an etching mask for the wet etching of a metal layer (*Cu*) on the *FPC*. First, the *FPC* was steeped in a ferric chloride solution and agitated by an ultrasonic cleaner for 9 min. After the etching process, the patterned *FPC* was cleaned and then dried by D.I. water and an N2 gun. Then, the distributed electrode on the *FPC* could be completed after being removed from the residual photoresist by acetone, as shown in Figs. 4(c) and (d).

iii. A blank *PVDF* film was prepared by stripping the Ag layers on both sides of a commercial *PVDF* film (Measurement Specialties Inc.) under acetone about 10 seconds, as referred to in Figs. 4(e) and (f).

iv. After the top and bottom *FPCs* had been patterned, a blank *PVDF* film was sandwiched by

Table 2 The specifications of the tactile sensor

Materials	Length (mm)	Width (mm)	Thickness (mm)
Bump-like structure (Silicone rubber)	5	5	2
Package layer (*PDMS*)	52.9	47.4	4
PVDF film	50.9	45.4	52×10^{-3}
FPC film	50.9	45.4	38×10^{-3}

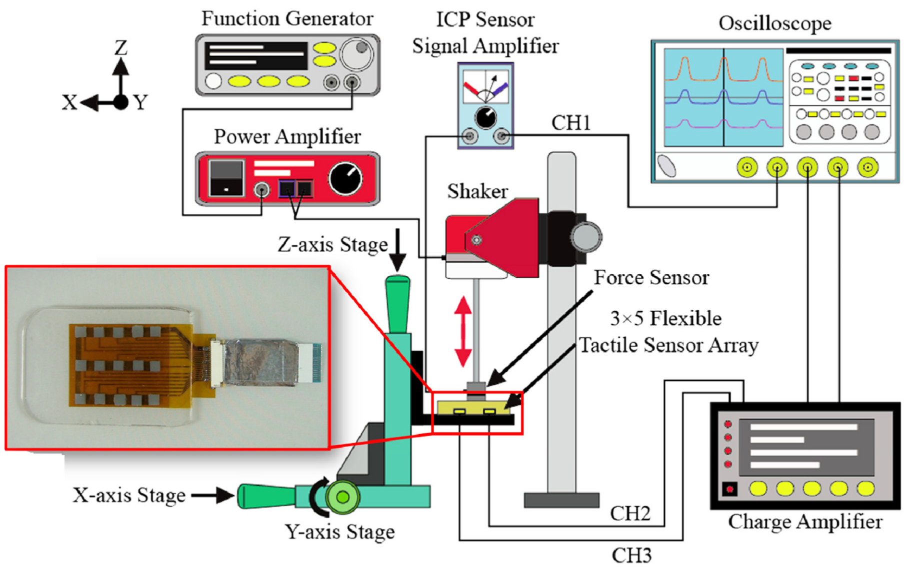

Fig. 5 The experimental setup for the characterization of sensor sensitivity and the finished 3×5 tactile sensor array

two *FPCs* with adhesive, as shown in Fig. 4(g).

v. The bump-like structures were fabricated using a molding technique. The master was made of PMMA fabricated using precision machining. Each bump-like structure was made of silicone rubber, as indicated in Figs. 4(h) and (i).

vi. 15 silicone rubber bump-like structures were molded onto the laminated *FPC* and aligned with the distributed electrodes and then the whole sensor was packaged with *PDMS* material in a mold. The tactile sensor was completed after curing the *PDMS* at 85°C for 30 min, as referred to in Figs. 4(j) and (k). The specifications of the finished tactile sensor are listed in Table 2 and shown in Fig. 5.

5. Experimental results and discussion

5.1 Characterization of tactile sensor

As regards a piezoelectric tactile sensor, it is difficult to measure a static force as the charges induced by a static force dissipate rapidly. Therefore, a dynamic testbed was built to characterize the performance of the piezoelectric-type tactile sensor, as shown in Fig. 5. The dynamic force was

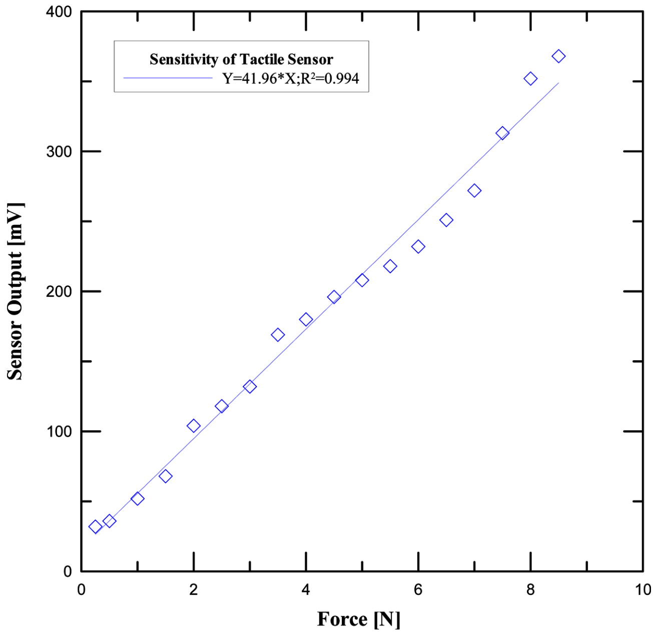

Fig. 6 Experimental results of sensor output shows the linearity between 0.2 to 9 N, and that its sensitivity is about 41.96 mV/N

given by a shaker (Data Physics Corp.) driven by a function generator (Agilent33220A) with a sinusoidal signal of 2 Hz. Additionally, a force sensor (PCB209C02, *PCB* Piezotronics, Inc.) was mounted in front of the shaker shaft for force calibration and taken as a reference for adjusting the amplitude of the shaker; the output signal of the force sensor was transmitted to the oscilloscope through channel 1 (CH1) for real-time monitoring. Thus, a periodic and calibrated force was generated and vertically acted on a single sensing element (taxel) of the tactile sensor. The output signal of the tactile sensor passed through a charge amplifier (B&K NEXUS2690A) to the oscilloscope's channel 2 (CH2) for signal acquisition. In the experiments, the output signal from the tactile sensor was not amplified, but a notch filter with a cutoff frequency of 60 Hz was employed for noise reduction from city power. By using a 3-axis stage, the shaker shaft could exactly act on the taxel where monitored by oscilloscope. Moreover, the applied force could be tuned by the input voltage from a function generator. As Fig. 6 shows, the relationship between the applied force and the output voltage of a single taxel had a good linearity of 0.2 N to 9 N. In addition, its sensitivity was about 42 mV/N as calculated by curve fitting. As far as we were able to tell, our tactile sensor possessed a higher sensitivity and lower detectable threshold force than the conventional thin-film electrode *PVDF* tactile sensor demonstrated by Yu *et al.* (2003). In Yu's work, the sensitivity and the threshold force were 0.2 mV/N and 0.7 N, respectively. Consequently, the structural electrode and soft packaging material used in this study not only improved the sensitivity, but also lowered the minimum detectable force of the piezoelectric tactile sensor. The weight of robot is 1.67 Kg (~16.3 N), therefore, the maximum loading for each foot is about 16.3 N as another foot suspended in the air. If the loading is evenly distributed on the 15 taxels; each taxel is in charge of about 1N, which is conformed to our sensing range (0.2 N~9 N). In addition, there is almost 9 times margin for the loading concentration as a robot walks in a rough surface. In general, our sensor was sufficiently satisfied with the requirement of a walking robot.

5.2 Foot pressure mapping system

The foot pressure mapping system comprised three parts: two 3×5 tactile sensor arrays of flexible tactile sensors; a readout circuit module for acquisition of the sensor outputs and transmitting signals to the computer; and the signal processing program for calculating the zero moment point and displaying a real-time pressure map on the computer screen. Two tactile sensors were attached to each foot of a biped robot, and the control box was placed on the robot's head and connected to the sensor and computer by a parallel interface and *USB*, respectively, as shown in Fig. 7. The readout circuit module included 30 *CMOS OP* amplifiers for each taxel, two 16-channel multiplexers connected with a 60 Hz notch filter and power amplifier, and a microcontroller (LM3S811, Texas Instruments Inc.) for *A*/*D* conversion and *I*/*O* signals between the sensor and computer, as shown in Fig. 7(c). The tactile sensor was first connected to a *CMOS OP* for magnifying the current signal in order to compensate for the low voltage output of the piezoelectric sensor which could easily lose its signal through transduction. Furthermore, the noise was also effectively reduced due to the *OP* having high input impedance and low output impedance for the impedance match between the piezoelectric sensor and the circuitry in the control box.

As regards the biped robot when walking, the foot mapping system scanned and transferred the

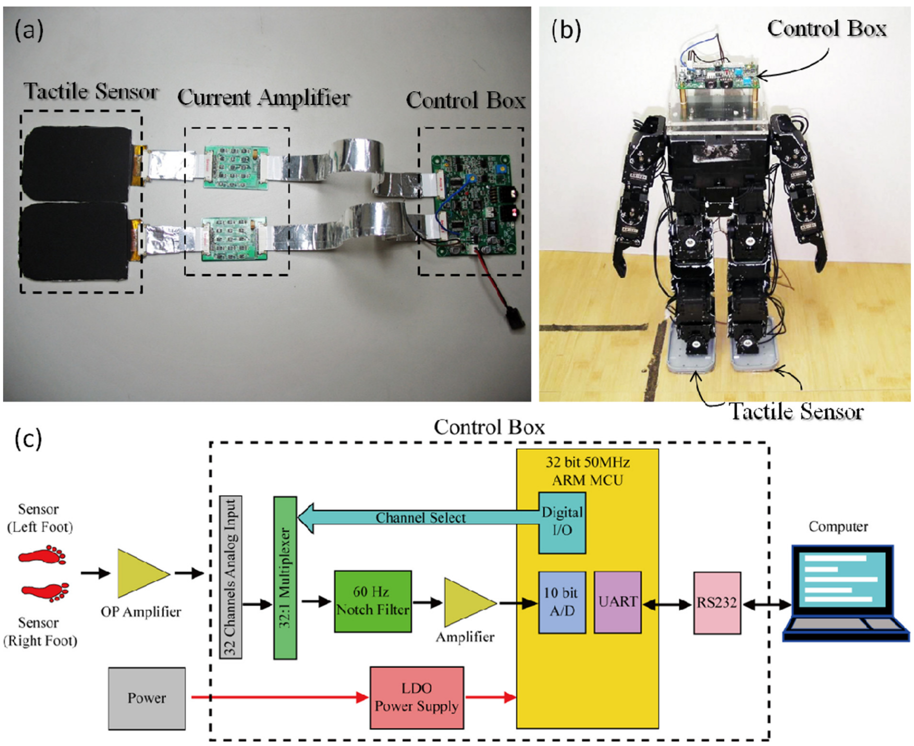

Fig. 7 (a) The photograph is of a read-out circuit module integrated with a tactile sensor, (b) two 3×5 tactile sensors were installed at the bottom of each biped-robot foot and the control box was mounted on the robot's head and (c) architecture of a readout circuit module output signals of the tactile sensor array to the connected computer via *USB*. Then, these signals were processed by a computer program (Shieh *et al.* 2012) for a real-time display of the pressure map and the calculation of the zero moment point. The location of the zero moment point can be denoted as *ZMP* ($\overline{X}, \overline{Y}$), where $\overline{X}$ and $\overline{Y}$ are the coordinates with respect to the origin point at the bottom left of the sensor array, as shown in Fig. 8(a). The calculation of the coordinates $\overline{X}$ and $\overline{Y}$ can be expressed by Eq. (1)

$$\overline{X} = \frac{\sum x_i \cdot \omega_i}{\sum x_i} \text{ and } \overline{Y} = \frac{\sum y_i \cdot \omega_i}{\sum x_i} \tag{1}$$

where x_i and y_i are the *x*-axis coordinate and y-axis coordinate of the i^{th} sensor, and ω_i is the pressure value of the i^{th} sensor. Therefore, when the computer program received the sensor output of each taxel, the pressure map was displayed on the screen, as well as the *ZMP* location. In this program, the refresh rate of each frame of pressure display was 0.8 ms and the maximum number of *ZMP* trajectories was 20 times in a cycle.

In order to easily recognize the distribution and magnitude of foot pressure, the pressure indicated in Fig. 6 was divided into 7 levels in different colors, as shown in Fig. 8(b). The bigger concentric circle indicates a higher pressure measured at that point, but the real pressure value of each taxel also can be seen in the same frame at the bottom. For example, the foot pressure maps of a real walking test for a biped robot can be seen in Fig. 8(c). The two foot pressure maps represent the left and right foot, respectively, and the location of the *ZMP* is indicated in the foot maps as a white spot. Hence, the trajectory of the *ZMP* could also be traced in this walking test.

In the simulation results, shown in Fig. 3, the cross-talk effect of the tactile sensor had to be avoided in order to identify the contact area. Thus, a proper spacing between the two structural electrodes and the segments of *PVDF* film was designed and fabricated for reducing the cross-talk effect. A knocking test was performed to demonstrate that there was no cross-talk effect in our foot

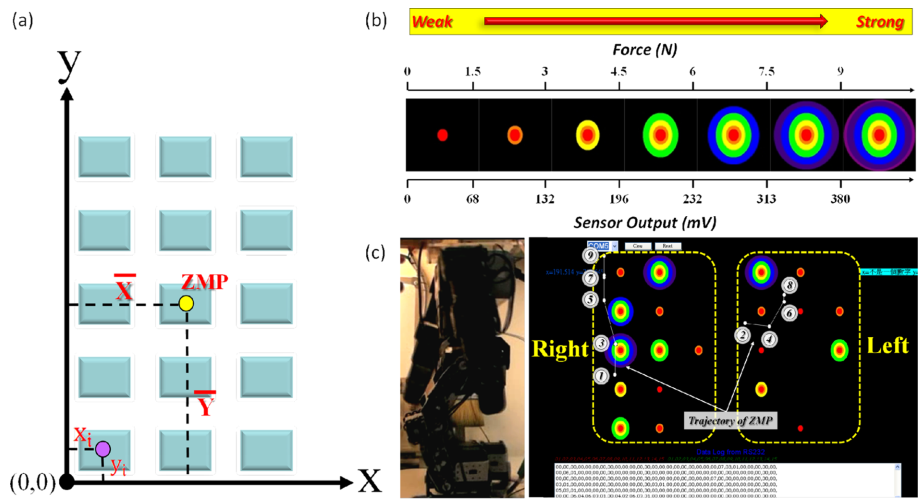

Fig. 8 (a) Location of zero moment point, *ZMP* ($\overline{X}, \overline{Y}$), with respect to the origin point at the left bottom of the 3 by 5 sensor array, (b) seven different levels for the magnitude of foot pressure displayed on the computer screen. and (c) two foot pressure maps of a walking test for a biped robot: the pressure of each taxel can be seen either in a symbolic display or the real value at the bottom

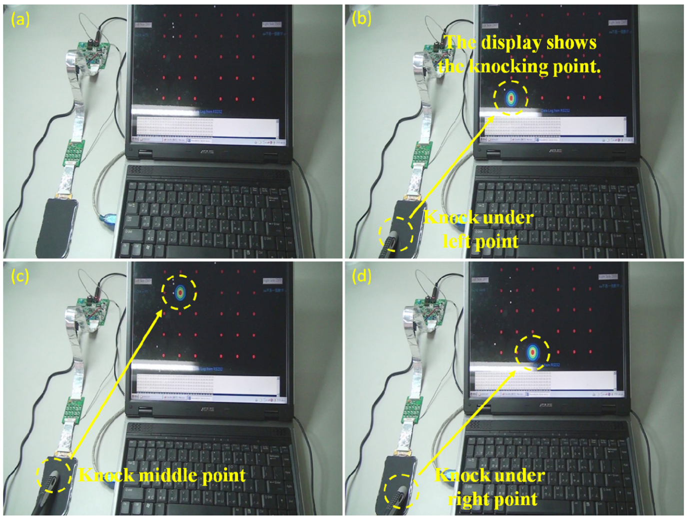

Fig. 9 Knocking test of the 3×5 tactile sensor, single knocking on the surface of tactile sensor by a pen. The pressure mapping results corresponding to the knocking test show the magnitude and distribution of the pressure on the computer screen. (a) experimental setup of knocking test, (b) knock at left point, (c) knock at middle point and (d) knock at right point

mapping system, as illustrated in Fig. 9. The sensor was knocked by a pen and the pressure magnitude and distribution were observed on the computer screen, with only the knocked point in the 3×5 taxels showing a pressure signal on the screen, while the untouched taxels generated no signal, as shown in Fig. 9(b). In addition, the knocking test was consistent for different taxels, as indicated in Figs. 9(c) and (d); consequently, the foot mapping system could feedback the reaction force of an uneven surface or obstacle in the walking path of a biped robot with 3×5 taxels in real time.

6. Conclusions

This study successfully developed a 3×5 flexible tactile sensor array and applied it to a biped robot with regards to foot pressure mapping. The novel tactile sensor introduced the concept of a structural electrode for sensitivity enhancement and the reduction of the cross-talk effect. By choosing a soft material for a packaging layer, sensitivity was enhanced to 42 mV/N, which was better than the conventional piezoelectric tactile sensor. The foot pressure mapping system was not only a real-time display of the dynamic pressure distribution and magnitude, but also provided the trajectory of the zero moment point when the robot was walking. Consequently, the foot mapping system could actually feedback the reaction force of an uneven surface or obstacle in the walking path of a biped robot. In the future, the system will be integrated with motion control for the biped robot, thus allowing a robot to adjust its posture in order to maintain its balance during motion.

Acknowledgments

The project was conducted successfully due to the much appreciated financial support of the

National Science Council of Taiwan (NSC 98-2221-E-218-023), and the Optoelectronics Research Center at Southern Taiwan University for the *MEMS* fabrication facilities.

References

Cavanagh, P.R., Hewitt, F.G. and Perry, J.E. (1992), "In-shoe plantar pressure measurement: a review", *The Foot*, **2**(4), 185-194.
Chuang, C.H., Dong, W.B. and Lo, W.B. (2008), "Flexible piezoelectric tactile sensor with structural electrodes array for shape recognition system", *Proceedings of the IEEE 3rd International Conference on Sensing Technology*, Tainan, Nov.
Chuang, C.H. (2009), *Flexible piezoelectric tactile sensor with structural electrodes array*, Recent Adv. In Sensing Technology, LNEE 49, 189-202. Springer.
Chuang, C.H., Lu, C.T. and Fang, T.H. (2009), "Slippage and direction sensing based on a flexible tactile sensor with structural electrodes", *Proceedings of the IEEE SENSORS 2009*, New Zealand, Oct.
Interlink Electronics Inc. (2011), On-Line, Available from Internet, http://www.interlinkelec.com/, accessed 23 May 2011.
Forner-Cordero, A., Koopman, H.J.F.M. and van der Helm, F.C.T. (2006), "Inverse dynamics calculations during gait with restricted ground reaction force information from pressure insoles", *Gait Posture*, **23**(2), 189-199.
Kalamdani, A.A. (2006), *Development and characterization of a high-spatial-temporal-resolution foot-solepressure measurement system*, Technical Report, CMU-RI-TR-06-38, Carnegie Mellon University, PA, Aug.
MacWilliams, B.A. and Armstrong, P.F. (2000), *Clinical applications of plantar pressure measurement in pediatric orthopedics*, A New Millennium in Clinical Care and Motion Analysis Technology on Pediatric Gait, NJ, April.
Mergner, T., Schweigart, G. and Fennell, L. (2008), "Vestibular humanoid postural control", *Physiology*, **103**(3-5), 178-194.
Park, J.H. (2003), "Fuzzy-logic zero-moment-point trajectory generation for reduced trunk motions of biped robots", *Fuzzy Set. Syst*., **134**(1), 189-203.
Qasaimeh, M.A., Sokhanvar, S., Dargahi, J. and Kahrizi, M. (2009), "*PVDF*-Based microfabricated tactile sensor for minimally invasive surgery", *J. Microelectromech. S*., **18**(1), 195-207.
Saito, N., Satoh, T. and Okano, H. (2006), "Grasping force control in consideration of translational and rotational slippage by a flexible sensor", *Proceedings of the IECON 32nd Annual Conference on IEEE Industrial Electronics*, Paris, Nov.
Tekscan Inc. (2011), On-Line, Available from Internet, http://www.tekscan.com/, accessed 23 May 2011.
Teshigawara, S., Ishikawa, M. and Shimojo, M. (2008), "Study of high speed and high sensitivity slip sensor characteristic of conductive material", *Proceedings of the SICE Annual Conference*, Tokyo, Aug.
Shieh, M.Y., Chen, C.S., Chuang, C.H., Liou ,Y.R. and Li, J.H. (2012), "Gait detection based stable locomotion control system for biped robots", *Comput. Math. Appl*., in press.
Vukobratovic, M. and Borovac, B. (2004), "Zero-moment point - thirty five years of its life", *Int. J. Hum. Robot*., **1**(1), 157-173.
Welton, E.A. (1992), "The Harris and Beath footprint: interpretation and clinical value", *Foot Ankle Int*., **13**(8), 268-462.
Woodbum, J. and Helliwell, P.S. (1997), "Observations on the *F*-Scan in shoe pressure measuring system", *Clin. Biomech*., **11**(5), 301-304.
Yip, S.W. and Prieto, T.E. (1996), "A system for force distribution measurement beneath the feet", *Proceedings of the 1996 15th Southern Biomedical Engineering Conference*, Dayton, Mar.
Yu, K.H., Yoon, M.J., Kwon, T.K. and Lee, S.C. (2003), "Distributed flexible tactile sensor system", *Int. J. Appl. Electrom*., **1-3**(18), 53-65.
Zhu, H., Maalej, N., Webster, J.G., Tompkins, W.J., Bach-y-Rita, P. and Wertsch, J.J. (1990), "An umbilical dataacquisition system for measuring pressures between the foot and shoe", *IEEET. Bio-Med. Eng*., **37**(9), 908-911.

CC